Contents lists available at ScienceDirect

Journal of Pipeline Science and Engineering

journal homepage: http://www.keaipublishing.com/en/journals/journal-of-pipeline-science-and-engineering/

# Prediction of properties on large diameter welded pipe: case study on 32″ × 16 mm X65 HSAW pipe

Steven Cooreman[a,*], Dennis Van Hoecke[a], Sandeep Abotula[b], Hervé Luccioni[c], Nikos Voudouris[d], Athanasios Tazedakis[d]

[a] ArcelorMittal Global R&D Gent/OCAS N.V., Pres. J. F. Kennedylaan 3, 9060 Zelzate, Belgium
[b] ArcelorMittal Global R&D East Chicago, 3001 East Columbus Drive, East Chicago, IN 46312, USA
[c] ArcelorMittal Europe – Flat Products, 13776 Fos-sur-Mer Cedex, France
[d] Corinth Pipeworks SA, VI.PE. Thisvis 320 10 Domvrena, Greece

ARTICLE INFO

*Keywords:*
Spiral pipe forming
Finite Element Modelling
Prediction of pipe properties
Levkovitch-Svendsen model
Kinematic hardening
Distortional hardening

ABSTRACT

Large diameter welded pipes are amongst the most cost-effective transportation means for oil and gas. The production of those pipes involves different cold forming steps, as a result of which the mechanical properties on pipe will be different from the plate or coil properties. The steel manufacturer has several parameters at hand to control the properties of his final product. However, the pipe manufacturer only has a narrow process window, but eventually he is responsible for the properties of his product, i.e. the pipe. Furthermore, for some pipeline applications, the properties in both the transverse and longitudinal pipe direction must be within certain limits. This paper presents a Finite Element model which allows simulating pipe forming and subsequent mechanical testing and thus could be adopted to predict pipe properties from coil/plate properties. The complex hardening behaviour exhibited by pipeline grades is described by an extended version of the Levkovitch-Svendsen model, a constitutive model which accounts for isotropic, kinematic and distortional hardening. To validate the model, numerical predictions were compared to experimental results obtained from mechanical tests conducted on 32″ × 16 mm X65 HSAW (Helical Submerged Arc-Welding) pipes. The properties on pipe were evaluated by means of ring expansion tests and tensile tests on (flattened) full-thickness dog-bone samples and non-flattened round bar samples. Furthermore, tensile tests were performed in the transverse and longitudinal pipe direction and tests were conducted before and after hydrotesting. In general, the numerical predictions are in good agreement with the experimental data.

## 1. Introduction

Large diameter welded pipes are one of the most cost-effective means for the transport of oil and gas. Despite the transition towards renewable energy sources, oil and gas will still be needed in the coming decades to fulfil the worldwide energy demand (International Energy Agency, 2020). Furthermore, large diameter welded pipes play an important role in our journey to a more durable energy infrastructure, e.g. for transport and storage of $CO_2$ (Di Biagio et al., 2018) and for transport of hydrogen (HyLINE, 2019; Gas For Climate, 2020).

In general, one can distinguish between Longitudinal Submerged Arc-Welding (LSAW), High Frequency Induction welding (HFI) and Helical Submerged Arc-Welding (HSAW) pipes. HSAW and HFI pipes are produced from coil by means of 3-roll bending and roll forming respectively, whereas LSAW pipes are produced from plate using UOE forming (Herynk et al., 2007), JCO forming (Chatzopoulou et al., 2017) or 3 or 4-roll bending. Those forming processes involve one or more cold deformation steps, each of which introduces plastic deformation.

Obviously, the mechanical properties on pipe must meet specific requirements in terms of toughness and strength, as indicated in international standards such as specification API 5L (API, 2018) from the American Petroleum Industry and standard ISO 3183 (ISO, 2007) from the International Standardization Organization. At the very least, the yield and tensile strength in $TD_{pipe}$ (transverse pipe direction) should be above a threshold value, referred to as SMYS (specified minimum yield strength) and SMTS (specified minimum tensile strength) respectively. Some applications, such as reel-lay installation (IOGP, 2019), also require the longitudinal properties on pipe to meet certain specifications, e.g. in terms of uniform elongation and yield to tensile strength ratio.

As pipe forming involves plastic deformation, the pipe properties will be different from the coil properties. Therefore, both steel producers and

* Corresponding author.
*E-mail address:* steven.cooreman@arcelormittal.com (S. Cooreman).

https://doi.org/10.1016/j.jpse.2022.100071
Received 6 May 2022; Received in revised form 31 May 2022; Accepted 12 June 2022

pipe makers would benefit from a tool which allows predicting pipe properties from coil/plate properties, because such a tool would help to define which coil/plate properties are required to reach the desired strength on pipe.

This paper presents an Finite Element (FE) model which makes it possible to simulate pipe forming in an efficient way. The model also allows reproducing the different types of mechanical tests which are used to evaluate the properties on pipe and, hence, could be used to predict pipe strength from coil/plate properties. An accurate description of the steel's hardening behaviour is key to obtain descent predictions of the pipe's yield and tensile strength. Line pipe grades - such as X65, X70 and X80 – exhibit a pronounced Bauschinger effect. Previous studies (Cooreman et al., 2016) have shown that combined kinematic-isotropic hardening models, which are by default available in commercial Finite Element Analysis (FEA) codes, can capture the Bauschinger effect and allow predicting properties in $TD_{pipe}$. However, it was observed that the properties in $LD_{pipe}$ (the longitudinal pipe direction) are largely underestimated when adopting such models. Therefore, it was decided to implement a more advanced constitutive model, which accounts for the change of shape of the yield surface with evolving plastic deformation. In general, this phenomenon is indicated as distortional hardening. In literature, several phenomenological models can be found which account for distortional hardening, e.g. the Homogenous Anisotropic Hardening (HAH) model proposed by Barlat et al. (2011) and the Levkovitch-Svendsen model (Levkovitch et al., 2007; Clausmeyer and Svendsen, 2015). While the HAH model only accounts for isotropic and distortional hardening, the Levkovitch-Svendsen model considers isotropic, kinematic and distortional hardening. In the present study, an extended version of the latter model was adopted.

Finally, a case study was conducted to assess the predictive capability of the FE model. X65 coil material, produced by ArcelorMittal Fos-sur-Mer, was transformed into 32″ × 16 mm HSAW pipe by Corinth Pipeworks (CPW). The properties on pipe were evaluated by means of ring expansion tests and tensile tests on (flattened) full-thickness dogbone and round bar samples (API, 2018). Furthermore, tensile tests were performed in the transverse and longitudinal pipe direction and tests were conducted before and after hydrotesting. The results of this case study are discussed in this paper.

## 2. HSAW pipe forming

Fig. 1 shows a schematic representation of CPW's HSAW pipe mill: after decoiling and levelling, the coil tail is welded to the coil head of the previous coil to make it a continuous process. Next, the coil edges are prepared for HSAW welding. Finally, the flat coil is transformed into a spiral pipe by means of 3-roll bending, during which inside tack welding is applied to secure the pipe's geometry. Next, the tack-welded pipe is moved to a separate welding stand, where inside and outside HSAW welding is applied to obtain a continuous helical weld. Afterwards, the HSAW weld is inspected by means of ultrasonic testing and X-ray. Finally, each pipe is subjected to a hydrotest to make sure that the pipe is watertight and to verify whether the pipe can withstand the internal pressure. During hydrotesting, the pipe is filled with water and pressurized so that the hoop stress in the pipe wall reaches a certain percentage of SMYS. This percentage typically varies between 80% and 100%. The pressure $p$ which must be applied during hydrotesting can be calculated as follows (ISO, 2007):

$$p = \frac{2\mathrm{WT} \cdot S}{\mathrm{OD}} \tag{1}$$

Where $p$ represents the internal pressure, WT the wall thickness, $S$ a certain percentage of SMYS and OD the outer pipe diameter.

The 32″ × 16 mm X65 HSAW pipes were produced from 1,450 mm wide coils with an inner diameter of 762 mm and an outer diameter of 2,008 mm. The pipe forming angle $\alpha$, i.e. the angle between coil rolling direction (RD) and $TD_{pipe}$, was 34.6°, as shown in Fig. 2.

In the case of X65 pipes, specified minimum yield strength in $TD_{pipe}$ (SMYS) equals 65 ksi or 448.16 MPa. The pipes were hydrotested at 90% of SMYS, meaning that an internal pressure of 16.2 MPa or 162 bar was applied.

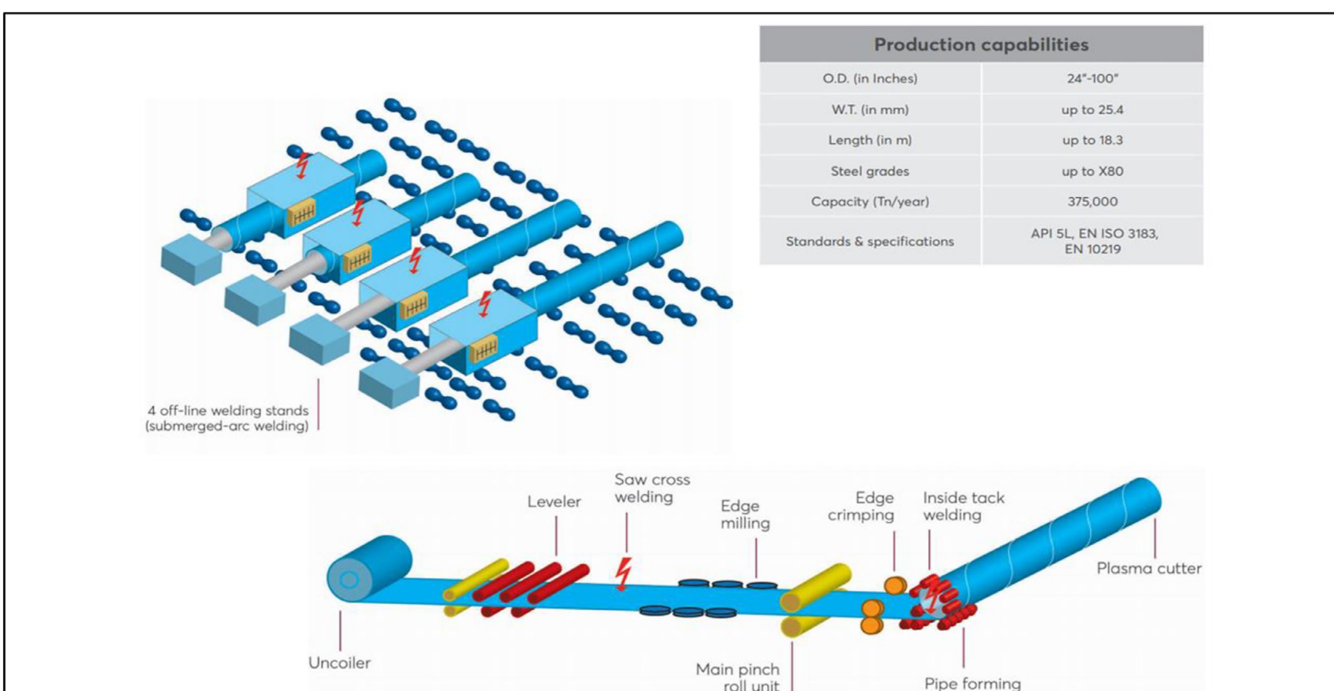


**Fig. 1.** CPW's HSAW pipe mill.

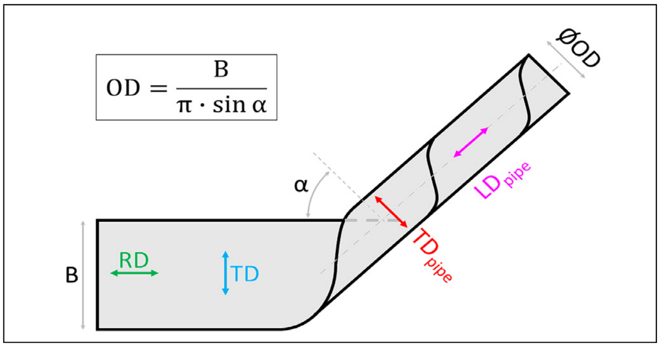


**Fig. 2.** HSAW pipe forming: relation between pipe forming angle $\alpha$, coil width $B$ and outer pipe diameter $D$ and indication of RD and TD, the rolling and transverse direction on coil, and $LD_{pipe}$ and $TD_{pipe}$, the longitudinal and transverse direction on pipe.

## 3. Mechanical testing of pipe

The pipe properties in $TD_{pipe}$ and $LD_{pipe}$ were evaluated by tensile testing full-thickness dog-bone and round bar samples (API, 2018). The yield strength in $TD_{pipe}$ was also measured by means of ring expansion tests (API, 2018). Tests were conducted at different positions along the coil length and before and after hydrotesting.

During ring expansion testing, 74.6 mm wide rings are expanded by means of internal pressure, while the circumferential elongation is measured. In the present study, the circumferential strain was measured by means of a chain extensometer, located at one of the edges, and an Linear Variable Differential Transformer (LVDT), positioned at mid width (Walsh et al., 2020). Only the average of both strain measurements is reported in the results section. Barlow's formula was used to calculate the circumferential stress in the pipe wall from the internal pressure:

$$\sigma = \frac{p \cdot \mathrm{OD}}{2\mathrm{WT}} \quad (2)$$

In general, OD is used to convert pressure to stress. However, the pressure is only working on the inner surface, so it would be more appropriate to use inner pipe diameter (ID).

The full-thickness dog-bone samples had a parallel length of 75 mm and a width of 38.1 mm and were tested on a servo-hydraulic 1,000 kN MTS machine, equipped with fatigue-rated wedge grips. Strain was measured at both Intrados and Extrados by means of a non-averaging clip-on extensometer with a gauge length of 50 mm, as shown in Fig. 3. Only the average of the Intrados and Extrados measurements is reported in the results section (Cooreman et al., 2014). The samples parallel with $TD_{pipe}$ were machined from 650 mm long strips which were flattened by means of 4-point bending. The samples were then taken from the flat central section (Cooreman et al., 2014; Cooreman et al., 2013).

The round bar samples had a parallel length of 32 mm and a diameter of 6.25 mm in the reduced section. Those samples were tested on a servo-hydraulic 250 kN MTS tensile machine. Strain was recorded with a clip-on extensometer with a gauge length of 25 mm. It should be noted that the position of the round bar samples was varied across the wall thickness: samples were taken as close as possible to either Intrados or Extrados.

## 4. FE pipe forming model

The FE modelling approach used to simulate HSAW pipe forming and subsequent mechanical testing is shown in Fig. 4. It was assumed that the different steps of the pipe forming process, except for hydrotesting, could be modelled as pure bending operations. Only the bending axis varies during the process: during decoiling and levelling bending occurs around TD, while spiral pipe forming and flattening can be modelled as bending around $LD_{pipe}$. Furthermore, the larger part of the coil width is deformed under plane strain conditions, where no straining occurs along the bending axis. Consequently, a rather simple FE model could be used to simulate spiral pipe forming. Such a model was developed in Abaqus/Implicit. Each forming step was simulated by means of a separate FE model, as shown in Fig. 4. However, the material state obtained at the end of a forming step, was imposed as initial condition in the next forming step to keep track of the deformation history. Only the central section of the coil width was modelled. Despite the fact that plane strain conditions were assumed, a 3D model was used. In this way it was possible to take into account the complete stress tensor and to avoid loss of information when transferring the material state from one process step to the next process step.

Additional FE models were developed to simulate mechanical testing after pipe forming and flattening. Depending on which material test was simulated, the material state obtained after either pipe forming, hydrotesting or flattening was imposed as initial condition.

## 5. Levkovitch-Svendsen model

### 5.1. Constitutive model

The Levkovitch-Svendsen model is an advanced constitutive model which accounts for isotropic, kinematic and distortional hardening and

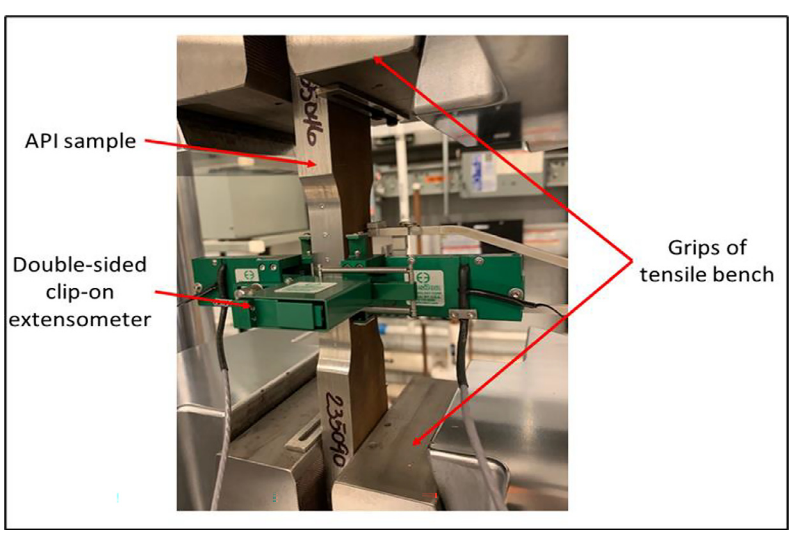


**Fig. 3.** When tensile testing the full-thickness dog-bone samples, a double-sided clip-on extensometer was used to record strain at Intrados and Extrados.

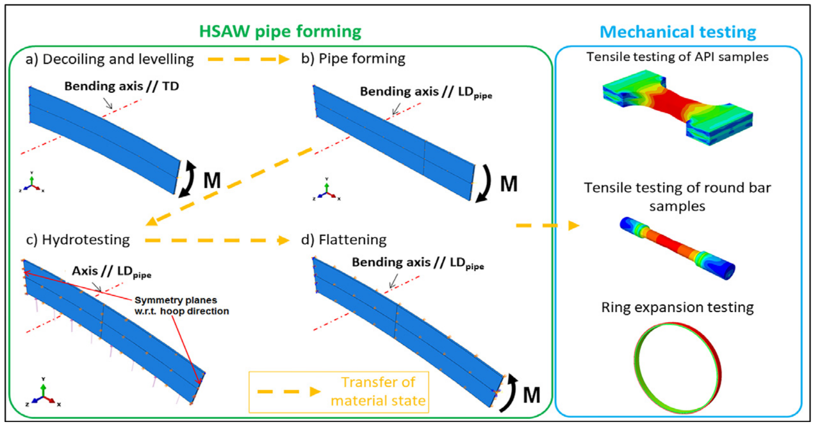


**Fig. 4.** FE model to simulate pipe forming and subsequent mechanical testing.

is thus able to capture phenomena such as the Bauschinger effect and cross-hardening (van Riel, 2009). A description of the original model can be found in Levkovitch et al. (2007). A slightly modified version was implemented by the authors.

The yield function takes the following form:

$$\Phi = \sigma_{\rm eq} + a\sigma_{ii} - \sigma_{\rm y} \le 0 \tag{3}$$

With $\sigma_{\rm eq}$ the equivalent stress, $\sigma_{ii}$ the trace of the Cauchy stress tensor $\boldsymbol{\sigma}$, $a$ a parameter governing the yield stress pressure sensitivity and $\sigma_{\rm y}$ the size of the yield surface. In the present study it was assumed that $a$ equals zero, meaning that the yield stress does not depend on hydrostatic pressure. The equivalent stress is defined as:

$$\sigma_{\rm eq} = \sqrt{\left(\boldsymbol{\sigma}^{\rm dev} - \boldsymbol{\alpha}^{\rm dev}\right) : (\boldsymbol{M} + \boldsymbol{H}) : \left(\boldsymbol{\sigma}^{\rm dev} - \boldsymbol{\alpha}^{\rm dev}\right)} \tag{4}$$

With $\boldsymbol{\sigma}^{\rm dev}$ the deviatoric part of the Cauchy stress tensor $\boldsymbol{\sigma}$, $\boldsymbol{\alpha}^{\rm dev}$ the deviatoric part of the backstress tensor $\boldsymbol{\alpha}$, $\boldsymbol{M}$ a fourth order tensor expressing the material's initial anisotropy and $\boldsymbol{H}$ a fourth order tensor which evolves with plastic deformation and describes the evolution of the material's anisotropy. In this study, the material's initial anisotropy was described by Hill's 1948 yield criterion (Hill, 1948).

As proposed by Chaboche et al. (1979), the total backstress $\boldsymbol{\alpha}$ is defined as a summation of different backstresses $\boldsymbol{\alpha}_k$, where the evolution of each backstress is defined by the Armstrong-Frederick model (Armstrong and Frederick, 1966):

$$\dot{\boldsymbol{\alpha}} = \sum_{k=1}^{N} \dot{\boldsymbol{\alpha}}_k \tag{5}$$

$$\dot{\boldsymbol{\alpha}}_k = C_k\left[\left(\frac{\sigma_{\rm eq}^{\rm Mises}}{\sigma_{\rm eq}^{\rm Work}}\right)^2 X_{{\rm sat},k}\boldsymbol{D}^{\rm pl} - \boldsymbol{\alpha}_k\dot{\varepsilon}_{\rm eq}^{\rm pl}\right] \tag{6}$$

With $N$ the number of backstresses, $C_k$ and $X_{{\rm sat},k}$ material parameters which must be calibrated based on mechanical tests, $\boldsymbol{D}^{\rm pl}$ the plastic strain rate tensor, $\dot{\varepsilon}_{\rm eq}^{\rm pl}$ the equivalent plastic strain rate, $\sigma_{\rm eq}^{\rm Mises}$ the equivalent von Mises stress and $\sigma_{\rm eq}^{\rm Work}$ the work-equivalent stress, which is defined as:

$$\sigma_{\rm eq}^{\rm Work} = \sqrt{\boldsymbol{\sigma}^{\rm dev} : \boldsymbol{M} : \boldsymbol{\sigma}^{\rm dev}} \tag{7}$$

In the present study, four backstress tensors were used to describe kinematic hardening to make sure that the model can accurately describe the cyclic stress-strain response and capture the pronounced Bauschinger effect exhibited by pipeline grades.

The distortional hardening tensor evolves as follows:

$$\dot{\boldsymbol{H}} = \dot{\varepsilon}_{\rm eq}^{\rm pl}C_{\rm D}\left[\left(\frac{\sigma_{\rm eq}^{\rm Work}}{\sigma_{\rm eq}^{\rm Mises}}\right)^2 D_{\rm sat} - H_{\rm D}\right]\boldsymbol{N}\otimes\boldsymbol{N} + \dot{\varepsilon}_{\rm eq}^{\rm pl}C_{\rm L}\left[L_{\rm sat}\left(\boldsymbol{I}^{\rm dev} - \boldsymbol{N}\otimes\boldsymbol{N}\right) - \boldsymbol{H}_L\right] \tag{8}$$

With $\boldsymbol{N}$ a second order tensor with Eucledian norm 1 and parallel with $\boldsymbol{D}^{\rm pl}$, $H_{\rm D}$ the projection of $\boldsymbol{H}$ on $\boldsymbol{N}\otimes\boldsymbol{N}$, $\boldsymbol{H}_{\rm L}$ the latent hardening part ($\boldsymbol{H}_{\rm L} = \boldsymbol{H} - H_{\rm D}\boldsymbol{N}\otimes\boldsymbol{N}$), $\boldsymbol{I}^{\rm dev}$ the deviatoric part of the fourth order unit tensor and $C_{\rm D}$, $L_{\rm sat}$, $C_{\rm L}$ and $D_{\rm sat}$ four material parameters which must be calibrated based on mechanical tests. As can be seen from Eqs. (6) and (8), the saturation parameters $X_{{\rm sat},k}$ and $D_{\rm sat}$ are scaled with a factor $(\sigma_{\rm eq}^{\rm Mises}/\sigma_{\rm eq}^{\rm Work})^2$ and $(\sigma_{\rm eq}^{\rm Work}/\sigma_{\rm eq}^{\rm Mises})^2$ respectively. By doing so, the amount of kinematic and directional hardening depends on the loading direction with respect to the principal material directions. Those scaling factors were not present in the original model. An explanation on why those scaling factors were introduced and how they were derived can be found in Cooreman and Coppieters (2021). The reader is referred to Levkovitch et al. (2007), Clausmeyer and Svendsen (2015) and Cooreman et al. (2018) for more details on the constitutive model.

### 5.2. Implementation in commercial FEA code

The model was implemented in Abaqus/Implicit (Dassault Systemes, 2020) by means of a UMAT user subroutine, using Voigt notation to improve the computational efficiency. Furthermore, a fully implicit backward Euler algorithm was applied to solve the set of nonlinear equations (Belytschko et al., 2000).

### 5.3. Calibration

A series of mechanical tests was conducted to calibrate the implemented Levkovitch-Svendsen model, more specifically tensile tests on full-thickness dog-bone and round bar samples in different directions, cyclic tension-compression tests with different strain amplitudes on round bar samples and torsion/tension and torsion/compression tests on tube-like samples (Fig. 5). The torsion/tension tests occurred in two stages: the samples were first loaded in torsion up to a certain strain level, unloaded and then loaded in either tension or compression or vice versa. Whereas the cyclic tension-compression tests allow quantifying the Bauschinger effect, the tension/torsion tests provide information on how the yield surface distorts with evolving plastic strain.

The graphs in Fig. 6 show the measured (solid, blue curve) and predicted (red, dashed curve) engineering stress-strain and torque-angle curves from some of the mechanical tests which were used to calibrate the constitutive model. As can be concluded from those graphs, the implemented Levkovitch-Svendsen model is capable of accurately describing the rather complex hardening behaviour of the X65 material considered in this study.

Tables 1–3 summarizes the calibrated values of the parameters of Hill's 1948 yield criterion and the kinematic and distortional hardening

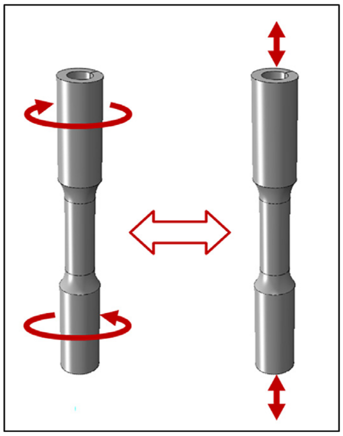

**Fig. 5.** Distortional hardening was quantified by means of torsion/tension and torsion/compression tests on tube-like samples. The samples were first loaded in torsion, unloaded and then loaded in either tension or compression or vice versa.

laws, while the green, solid curve in Fig. 7 indicates how the size of the yield surface $\sigma_y$ evolves as a function of the equivalent plastic strain $\varepsilon_{eq}^{pl}$. As can be observed from this graph, the yield surface shrinks during initial plastic deformation.

## 6. Results and discussion

The graph in Fig. 8 gives an overview of the coil and pipe yield ($R_{t0.5}$, i.e. engineering stress at a total strain of 0.5%) and tensile ($R_m$) strength, as measured by means of ring expansion testing and tensile testing of (flattened) full-thickness dog-bone samples and round bar samples. The colored bars indicate the average values, while the error bars indicate the minimum and maximum values. For the coil material, only the properties in the transverse direction (TD) are reported. It should be mentioned that the coil properties were measured at the coil tail, which is typically somewhat stronger than the remainder of the coil. In the case of the pipe material, the yield and tensile strength in the transverse ($TD_{pipe}$) and longitudinal ($LD_{pipe}$) pipe direction are reported (see Fig. 2). The SMYS is also plotted in this graph.

For all tests, the yield strength in $TD_{pipe}$ is above SMYS. The difference in yield strength between tests on flattened full-thickness dog-bone samples and ring expansion tests is quite small; on average, the ring expansion tests provide 10 MPa higher yield strength values than the tests on the flattened samples. However, it was observed that the rings get a conical shape during ring expansion testing, as a result of which the yield strength obtained from the LVDT measurement was around 20 MPa higher than the value obtained from the chain extensometer. Furthermore, when testing the rings which were taken from the hydrotested pipes, one of the seals failed before the LVDT extensometer reached 0.5% of strain. It could not yet be determined why the rings get conical. However, as this was the case for all tested rings, it seems to indicate a test artefact. Preliminary investigations by means of FE modelling have shown that it may be a problem of friction. If this would be the case, the actual $R_{t0.5}$ values, as measured by means of ring expansion testing, would be higher than the values reported in Fig. 8.

The yield strength in $TD_{pipe}$, as measured by means of tensile tests on round bar samples, shows quite some variation. As mentioned before, round bar samples were taken close to either Intrados or Extrados. It can be expected that the samples taken close to Intrados will provide rather low yield strength values, because those samples were taken

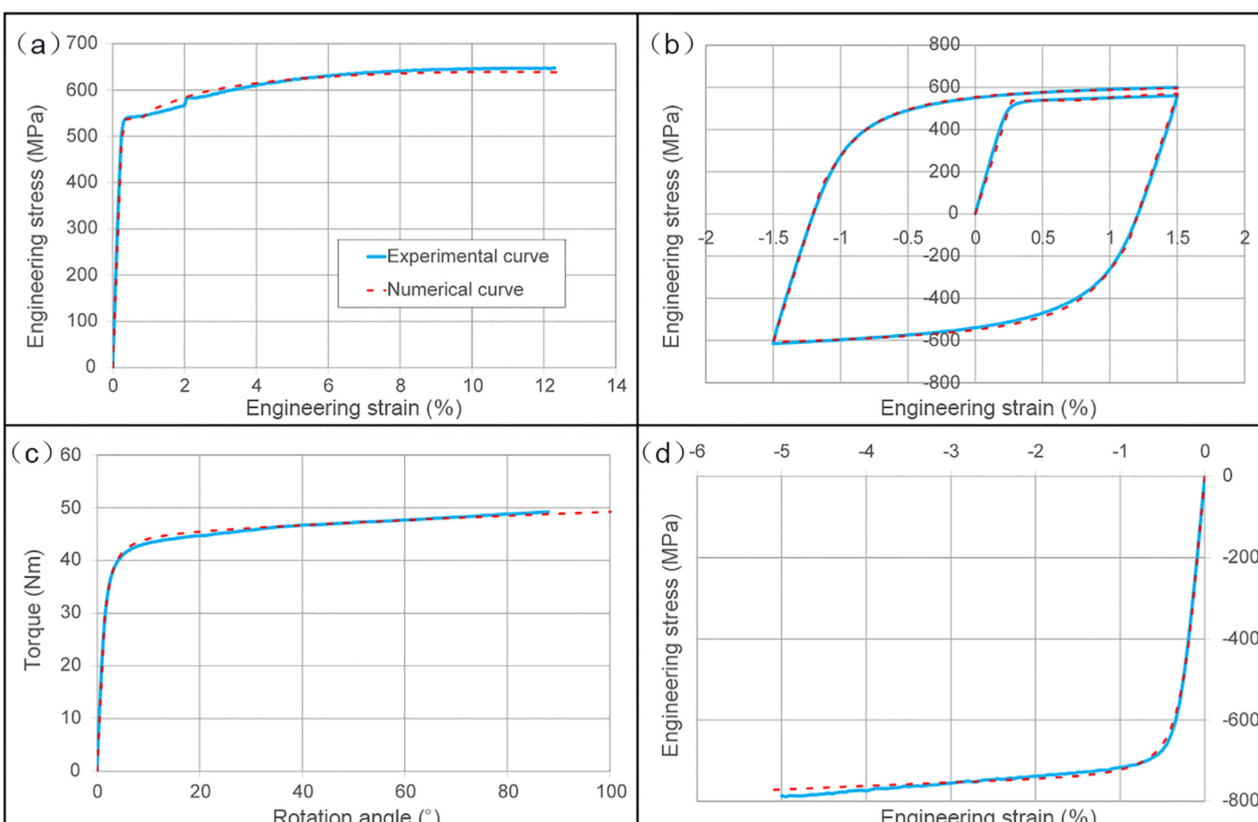


**Fig. 6.** Stress-strain and torque-rotation curves from some of the mechanical tests which were used for calibrating the constitutive model. a) Uniaxial tensile test in TD, b) Cyclic tension-compression test in TD with a strain amplitude of 1.5%, c) Torsion around TD after uniaxial tension in TD to 3%, d) Uniaxial compression in TD after torsion around TD to 45°. The blue, solid curve represents the measured curve, while the red, dashed curve represent the predicted curve.

**Table 1**
Model parameters of Hill 1948 yield criterion.

| $F$ | $G$ | $H$ | $M$ | $N$ | $L$ |
|---|---|---|---|---|---|
| 0.47 | 0.45 | 0.53 | 1.60 | 1.5 | 1.53 |

**Table 2**
Model parameters of kinematic hardening law.

| $X_{sat,1}$ (MPa) | $C_1$ | $X_{sat,2}$ (MPa) | $C_2$ | $X_{sat,3}$ (MPa) | $C_3$ | $X_{sat,4}$ (MPa) | $C_4$ |
|---|---|---|---|---|---|---|---|
| 62.6 | 311.2 | 56.2 | 1006.8 | 41.1 | 75.7 | 77.3 | 11.2 |

**Table 3**
Model parameters of distortional hardening law.

| $D_{sat}$ | $C_d$ | $L_{sat}$ | $C_l$ |
|---|---|---|---|
| 1.70 | 14.50 | -0.30 | 65.23 |

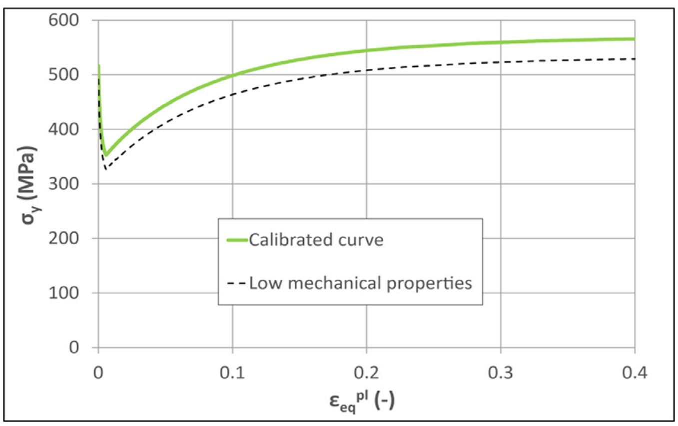


**Fig. 7.** Evolution of the size of the yield surface ($\sigma_y$) as a function of the equivalent plastic strain ($\varepsilon_{eq}^{pl}$). The green, solid curve represents the calibrated curve. The black, dashed curve was also considered in the numerical study (see Section 6) to account for the variation of mechanical properties along the coil length.

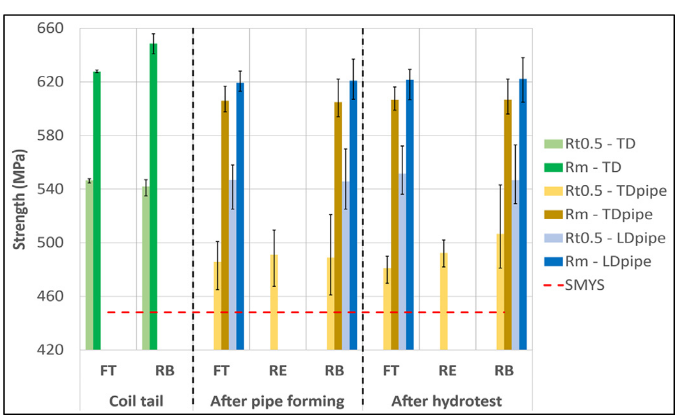


**Fig. 8.** Summary of experimental results: overview of coil and pipe properties, as determined by ring expansion testing (RE) and tensile testing of (flattened) full-thickness (FT) dog-bone samples and round bar (RB) samples.

from a region which was deformed in compression during pipe forming. Thus, those samples will suffer from the Bauschinger effect, as they are subjected to a load reversal when tested. The samples taken close to Extrados, on the other hand, contain less material from the compressed region and will thus provide higher yield strength values.

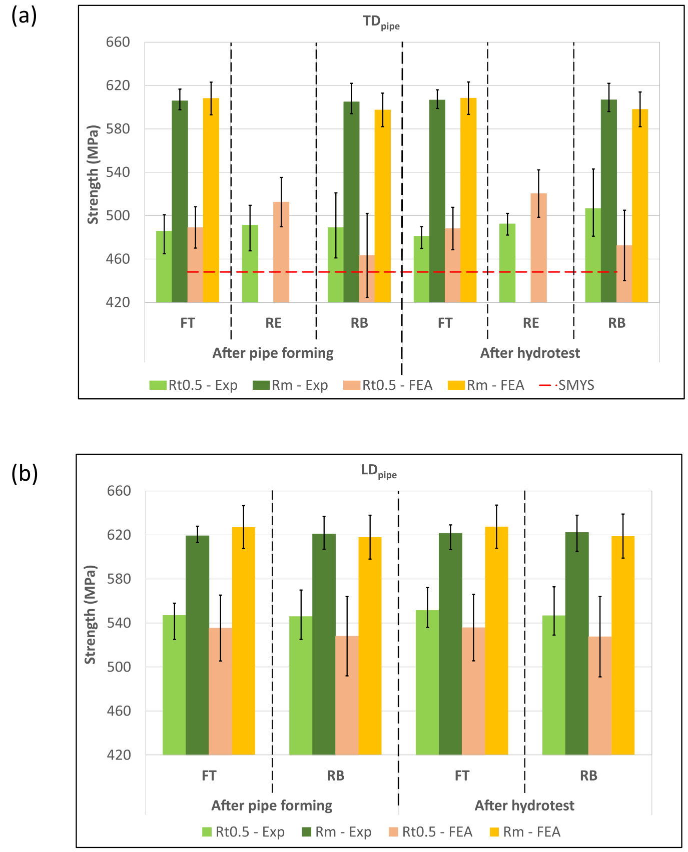


**Fig. 9.** Comparison between experimental measurements and predicted values: a) yield and tensile strength in $TD_{pipe}$, b) yield and tensile strength in $LD_{pipe}$ (FT: (flattened) full-thickness dog-bone sample, RB: round bar sample, RE: ring expansion test).

For all tests, one can observe that the yield strength in $LD_{pipe}$ is much higher than the yield strength in $TD_{pipe}$, while the difference in tensile strength is very limited.

The effect of hydrotesting seems to be negligible, except for the yield strength in $TD_{pipe}$ as resulting from tensile tests on round bar samples, where the yield strength increases, on average, around 15 MPa because of hydrotesting.

The graphs in Fig. 9 compare the pipe properties predicted by the FE model to the measured yield and tensile strength values. The colored bars indicate the average values while the error bars indicate the minimum and maximum values.

The Levkovitch-Svendsen model was calibrated based on tests conducted on samples taken from the coil tail. To account for the variation of mechanical properties along the coil length and given the fact that the coil tail is typically somewhat stronger than the remainder of the coil, simulations were run for two levels of mechanical properties: one time with the calibrated set of material parameters and another time with a set of parameters which predicts a 25 MPa lower yield and tensile strength on coil (black, dashed curve in Fig. 7).

For what concerns the yield strength in $TD_{pipe}$ and $LD_{pipe}$ as measured by means of tensile tests on (flattened) full-thickness dog-bone samples, the model predictions are in good agreement with the experimental data.

The model seems to overestimate the yield strength obtained from ring expansion testing. However, in the FE model it was assumed that the residual stresses present in the pipe wall after pipe forming are perfectly balanced. Ring split tests conducted on the actual pipes showed that the residual stresses were not balanced, as the pipe rings showed some opening when cut in the longitudinal direction. It can be expected that the model predictions would be around 10 MPa lower if the unbalance of residual stresses would be taken into account. Furthermore, as discussed above, the setup which was used for ring expansion testing seems to have a problem, as a result of which the measured $R_{t0.5}$ values underestimate the actual yield strength.

In the case of the round bar samples, the model seems to underestimate the yield strength in $TD_{pipe}$. However, one should keep in mind that, in reality, samples cannot be taken as close to Intrados and Extrados as in the FE model. This will particularly affect the yield strength obtained from the Intrados samples, because taking the samples somewhat further away from the Intrados side, may result in a significantly higher yield strength. Furthermore, in general, mechanical properties slightly vary across the thickness; it can be expected that the material close to the surface is somewhat stronger than the material at mid thickness. This variation is not considered in the FE model.

## 7. Conclusions

This paper presents an FE model, which allows simulating pipe forming and subsequent mechanical testing and thus could be adopted to predict pipe properties from coil properties. The FE model makes use of the Levkovitch-Svendsen model to describe the rather complex hardening behaviour of pipeline grades. This constitutive model accounts for isotropic, kinematic and distortional hardening and was further extended to obtain a more accurate description of the cyclic stress-strain response and the Bauschinger effect.

To validate the FE model, an extensive experimental study was conducted on 32″ × 16 mm X65 HSAW pipes. The mechanical properties on pipe were evaluated in detail by conducting ring expansion tests and tensile tests on round bar and (flattened) full-thickness dog-bone samples. In addition, an extensive set of tests on samples taken from coil was performed to calibrate the constitutive model.

The FE pipe forming model was then used to simulate forming of the 32″ × 16 mm X65 pipes and subsequent mechanical testing and the model predictions were compared to the experimental data. In general, the numerical predictions are in good agreement with the experimental data, both for the properties in $TD_{pipe}$ and $LD_{pipe}$.

## Declaration of Competing Interest

The authors declare that they have no known competing financial interests or personal relationships that could have appeared to influence the work reported in this paper.

## Acknowledgements

This research did not receive any specific grant from funding agencies in the public, commercial, or not-for-profit sectors.

## Supplementary materials

Supplementary material associated with this article can be found, in the online version, at doi:10.1016/j.jpse.2022.100071.

## References

API, 2018. Line pipe: API Specification 5L, 46th Edition Ameriacna Petroleum Institute.
Armstrong, P., Frederick, C., 1966. A mathematical representation of the multiaxial bauschinger effect: G.E.G.B. Report RD/B/N, 731.
Barlat, F., Gracio, J., Lee, M.-G., Rauch, E., Vincze, G., 2011. An alternative to kinematic hardening in classical plasticity. Int. J. Plast. 27, 1309–1327. doi:10.1016/j.ijplas.2011.03.003.
Belytschko, T., Liu, W., Moran, B., 2000. Nonlinear finite elements for continua and structures. Wiley & Sons, Sussex, England.
Chaboche, J.L., Dang Van, K., Cordier, G., 1979. Modelization of the strain memory effect on the cyclic hardening of 316 stainless steel. In: Proceedings of the 5th International Conference on Structural Mechanics in Reactor Technology, Division L11/3. Berlin, Germany August 13-17.
Chatzopoulou, G., Antoniou, K., Karamanos, S.A., 2017. Numerical simulation of JCO pipe forming process and its effect on the external pressure capacity of the pipe. In: Proceedings of the 36th International Conference on Ocean, Offshore and Arctic Engineering (OMAE 2017). Trondheim, Norway June 25-30.
Clausmeyer, T., Svendsen, B., 2015. Comparison of two models for anisotropic hardening and yield surface evolution in bcc sheet steels. Eur. J. Mech. A/Solids 54, 120–131. DOI: 10.1016j.euromechsol.2015.05.016.
Cooreman, S., Coppieters, S., 2021. On solving inconsistencies between different types of hardening models. In: Proceedings of XVI International Conference on Computational Plasticity. Fundamentals and Applications. COMPLAS 2021. Barcelona, Spain September 7-9.
Cooreman, S., Van Hoecke, D., Liebeherr, M., Thibaux, P., 2013. Measurement of mechanical properties on line pipe: difficulties and pitfalls. In: Proceedings of the 6th International Pipeline Conference. Ostend, Belgium October 6-9.
Cooreman, S., Van Hoecke, D., Liebeherr, M., Thibaux, P., Yamaguti-Enderlin, M., 2014. Measurement of mechanical properties on line pipe: comparison of different methodologies. In: Proceedings of the 10th International Pipeline Conference (IPC2014). Calgary, Alberta, Canada September 29-October 3.
Cooreman, S., Van Hoecke, D., Liebeherr, M., Thibaux, P., Yamaguti-Enderlin, M., 2016. Experimental and numerical study on the evolution of mechanical properties during spiral pipe forming. In: Proceedings of the 11th International Pipeline Conference (IPC2016). Calgary, Alberta, Canada September 26-30.
Cooreman, S., Van Hoecke, D., Liebeherr, M., Thibaux, P., Luccioni, H., 2018. Advanced constitutive model for the accurate evaluation of the structural performance of welded pipes in offshore applications. In: Proceedings of the 12th International Pipeline Conference (IPC2018). Calgary, Alberta, Canada September 24-28.
Dassault Systemes, 2020. Abaqus user subroutines Guide. ABAQUS Inc, Providence, USA.
Di Biagio, M., Spinelli, C., Brauer, H., et al., 2018. Requirements for safe and reliable $CO_2$ transportation pipeline ($SARCO_2$): final report. European Commission, Directrorate General for Research and Innovation. https://data.europa.eu/doi/10.2777/205449.
Gas For Climate, 2020. European hydrogen backbone. https://gasforclimate2050.eu/ehb/. 2020.
Herynk, M.D., Kyriakides, S., Onoufriou, A., Yun, H.D., 2007. Effects of the UOE/UOC pipe manufacturing processes on pipe collapse pressure. Int. J. Mech. Sci. 49, 533–553.
Hill, R., 1948. A theory of the yielding and plastic flow of anisotropic metals. Proceedings of Royal Society of London May 27th.
HyLINE, 2019. Safe pipelines for hydrogen transport. https://www.sintef.no/en/projects/hyline-safe-pipelines-for-hydrogen-transport/ (accessed 18 December 2020).
International Energy Agency, 2020. World energy outlook. https://www.iea.org/reports/world-energy-outlook-2020 (accessed 15 December 2020).
IOGP, 2019. Supplementary Specification to API Specification 5L and ISO 3183 Line Pipe: IOGP S-616. IOGP Specification S-616. IOGP.
ISO, 2007. Petroleum and natural gas industries - Steel pipe for pipeline transportation systems: ISO 3183.
Levkovitch, V., Svendsen, B., Aydin, M., Kessler, L., 2007. Accurate hardening modeling as basis for the realistic simulation of sheet forming processes with complex strain-path changes. LS-Dyna Anwenderforum, Frankenthal, Germany October 11-12.
van Riel, M., 2009. Strain path dependency in sheet metal - Experiments and models. Universiteit Twente, The Netherlands PhD thesis.
Walsh, W., Abotula, S., Konda, B., 2020. Ring expansion testing innovations: hydraulic clamping and strain measurement methods. In: Proceedings of the 13th International Pipeline Conference (IPC2020). Calgary, Alberta, Canada September 28-October 2.